Confinement Factors and Modal Volumes of Micro- and Nanocavities Invariant to Integration Regions

Shu-Wei Chang, *Member, IEEE*

***Abstract*—We present a convenient and self-consistent approach to calculate confinement factors and modal volumes of micro- and nanocavities, which are important for ultrasmall lasers and cavity quantum electrodynamics. This scheme does not rely on the numerical integrations related to optical fields and can avoid the indefinite dependence of physical quantities on integration regions. As a result of this built-in invariance to integration regions, the field representation of the confinement factor, in additional to its conventional expression, contains counter terms of volume and surface integrals, which cancel the effect of arbitrary integration volumes. This procedure is useful for small open cavities or those without sharp boundaries that distinguish cavity regions from free spaces. The uncertainty from different choices of integration regions can be thus eliminated.**

***Index Terms*—Confinement factor, microcavity, microlaser, modal volume, nanocavity, nanolaser.**

I. Introduction

THE confinement factor of a laser cavity is one of the important parameters which characterize the lasing performance. This quantity indicates how well the lasing mode profile overlaps with the active region where the gain medium is present. In a waveguide, the confinement factor is expressed as the ratio between two cross-sectional integrals of fields: one in the active area, and the other throughout the whole waveguide cross section [1]–[6]. If the lasing mode is a guided mode, the confinement factor calculated in this way is usually well defined. For 3-D cavities, the generic expression of confinement factors Γ is often written in an analogous form to the waveguide counterpart as [2], [7]–[9]

$$\Gamma = \frac{\int_{\Omega_\mathrm{a}} \mathrm{d}\mathbf{r}[\cdots|\mathbf{E}(\mathbf{r})|^2]}{\int_{\Omega} \mathrm{d}\mathbf{r}[\cdots|\mathbf{E}(\mathbf{r})|^2 + \cdots|\mathbf{H}(\mathbf{r})|^2]} \tag{1}$$

where Ω_a and Ω are the active region and an integration region (often set to the whole computation domain), respectively; $\mathbf{E}(\mathbf{r})$ and $\mathbf{H}(\mathbf{r})$ are the electric and magnetic field profiles, respectively; and "$\cdots$" represents some physical quantity such as the permittivity or permeability, depending on details of formulations. The expression in (1) has been utilized in numerical calculations for different cavity structures [7], [9]–[12] and often leads to reasonable values.

The appearance of confinement factors in (1) is, nevertheless, loosely defined. Suppose that far away from the cavity region is the lossless free space. If we adopt an integration region extending to the far-field zone so that the laser at the steady state can be approximated as a localized source, the far-field approximation indicates that magnitudes of optical fields exhibit an asymptotic behavior of the inverse distance r from the cavity region [13]:

$$\lim_{r\to\infty}|\mathbf{E}(\mathbf{r})| = \frac{f_\mathrm{e}(\theta,\phi)}{r} \quad \lim_{r\to\infty}|\mathbf{H}(\mathbf{r})| = \frac{f_\mathrm{h}(\theta,\phi)}{r} \tag{2}$$

where θ and ϕ are the polar and azimuthal angles of the coordinate; and $f_\mathrm{e}(\theta,\phi)$ and $f_\mathrm{h}(\theta,\phi)$ are the far-field patterns of $\mathbf{E}(\mathbf{r})$ and $\mathbf{H}(\mathbf{r})$, depending on the multipole expansion of the equivalent source to the lasing near field. If we choose the integration region Ω as a ball with a radius R_b much larger than the lasing wavelength and keep in mind that the differential volume $\mathrm{d}\mathbf{r} = r^2\sin\theta\mathrm{d}r\mathrm{d}\theta\mathrm{d}\phi$ has the r^2 dependence, the denominator of Γ in (1) becomes

$$\begin{aligned}&\int_\Omega \mathrm{d}\mathbf{r}[\cdots|\mathbf{E}(\mathbf{r})|^2 + \cdots|\mathbf{H}(\mathbf{r})|^2]\\ &\approx \int_0^{R_\mathrm{c}}\mathrm{d}r[\cdots] + \int_{R_\mathrm{c}}^{R_\mathrm{b}}\mathrm{d}r\int_0^{2\pi}\mathrm{d}\phi\int_0^{\pi}\mathrm{d}\theta\sin\theta\\ &\quad\times\left[\cdots|f_\mathrm{e}(\theta,\phi)|^2 + \cdots|f_\mathrm{h}(\theta,\phi)|^2\right] \propto R_\mathrm{b} = \mathrm{O}(\mathrm{V}^{1/3})\end{aligned} \tag{3}$$

where R_c is a phenomenological cutoff radius above which the far-field approximation is applicable; and V is the volume of Ω. In (3), we drop the radial integral below R_c since it does not scale with R_b. For a given active region Ω_a, the integral of the numerator in (1) is a fixed number. Therefore, the confinement factor Γ scales as $V^{-1/3}$ and ultimately vanishes as $V\to\infty$. As a result, the expression in (1) is improperly defined. Specific constraints which bypass this flaw such as carrying out the integral in (3) in the minimal ball outside which the field is solely composed of outgoing waves [14] were attempted. Common numerical schemes such as the finite-difference-time-domain (FDTD) method [7], [9], [10], [12] and complex-frequency (complex-ω) method [7], [15] bare similar problems. In particular, field integrations in the complex-ω method are more involved due to divergent far fields [16], [17].

The nonphysical scaling of the confinement factor with the size of integration region originates from the far-field contribution irrelevant to the lasing action. From this viewpoint, one

Manuscript received December 30, 2011; revised March 22, 2012; accepted March 28, 2011. This work was sponsored in part by the research project of Research Center for Applied Sciences, Academia Sinica, Nankang, Taipei, Taiwan, and in part by the National Science Council, Taiwan, under Contract NSC100-2112-M-001-002-MY2.

The author is with the Research Center for Applied Sciences, Academia Sinica, Nankang, Taipei 11529, Taiwan, and also with the Department of Photonics, National Chiao-Tung University, Hsinchu 30010, Taiwan (e-mail: swchang@sinica.edu.tw).

Color versions of one or more of the figures in this paper are available online at http://ieeexplore.ieee.org.

Digital Object Identifier 10.1109/JSTQE.2012.2193119

would attempt to adopt an integration region that does not extend too much outside the cavity region to exclude the unnecessary contribution from the far field. However, it is not straightforward to construct such an integration region so that only the field relevant to the lasing action is included in the confinement factor. This is especially true for small cavities with low radiative quality Q factors since the lasing mode may easily leak into the free space. Alternatively, an expression of the confinement factor invariant to integration regions would be more useful.

In this paper, we present a convenient and self-consistent approach to calculate the confinement factor. In addition, we also calculate two types of modal volumes. One is used in the laser rate equations [8], and the other is often adopted in the cavity quantum electrodynamics (cavity QED) [15] and Purcell effect [18]. This method is based on a frequency-domain formulation for reciprocal cavities [17], which has been applied to experimental data of real devices with satisfactory agreements [19]. An analogous procedure was described in [20] from the viewpoint of permittivity-induced variations of cavity resonances and examined with the complex-ω method. For the approach presented here, we derive a representation of the confinement factor in terms of various field integrals and show that in addition to the conventional expression in (1), extra counter terms of volume and surface integrals are present so that the physical confinement factor does not depend on integration regions. This situation is analogous to cancellations of infinities for key parameters in the quantum field theory: even though renormalized quantities do depend on the energy scale of detections, their seeming divergences due to path integrals are eliminated by the counter terms in the Lagrangian [21]. As an example, we calculate the confinement factors and modal volumes of whispering gallery modes (WGMs) in a dielectric sphere and show how the indefiniteness of the expression in (1) shows up as the integration region becomes larger.

The main factor leading to a physical confinement factor in this approach lies in that the photon lifetime, which is proportional to the Q factor, and threshold gain are simultaneously obtained in a physical manner [17]. Other schemes such as the FDTD and complex-ω methods can provide the photon lifetime or Q factor but could not access the threshold gain directly. In those methods, the threshold gain is obtained either from the region-dependent integration of the confinement factor (the original problem) or insertions of different gain coefficients into the active region in search of a value at which the photon lifetime or Q factor of the warm cavity approaches infinity [7], [9]. Thus, the procedure presented here is a convenient and physical modeling tool for small lasers, particularly those with low radiative Q factors or without clear borders between cavities and free spaces.

II. Confinement Factor as the Balance Measure between Gain and Loss

We consider the *energy confinement factor* $\Gamma_{\mathrm{E},l}$ of mode l, which is closely related to the electromagnetic energy in the dispersive but nonmagnetic material [8], [22]. Without the spontaneous-emission term in the rate equation of the photon density, the threshold condition of mode l is

$$\frac{1}{\tau_{\mathrm{p},l}} = \frac{\omega_l}{Q_l} = \Gamma_{\mathrm{E},l} v_{\mathrm{g,a}}(\omega_l) g_{\mathrm{th},l} \tag{4}$$

where $\tau_{\mathrm{p},l}$ is the photon lifetime; ω_l is the resonance frequency of mode l; Q_l is the quality factor; $v_{\mathrm{g,a}}(\omega_l)$ is the material group velocity of the gain medium; and $g_{\mathrm{th},l}$ is the threshold material gain. The material group velocity is inversely proportional to the material group index $n_{\mathrm{g,a}}(\omega_l)$ in the active region, which is related to the frequency derivative of the refractive index $n_{\mathrm{a}}(\omega) \approx \sqrt{\epsilon_{\mathrm{a,R}}(\omega)}$ at ω_l [8]:

$$v_{\mathrm{g,a}}(\omega_l) = \frac{c}{n_{\mathrm{g,a}}(\omega_l)} \tag{5a}$$

$$n_{\mathrm{g,a}}(\omega_l) = \left.\frac{\partial[\omega n_{\mathrm{a}}(\omega)]}{\partial\omega}\right|_{\omega=\omega_l} \approx \frac{[\epsilon_{\mathrm{g,a}}(\omega_l) + \epsilon_{\mathrm{a,R}}(\omega_l)]}{2n_{\mathrm{a}}(\omega_l)} \tag{5b}$$

where $\epsilon_{\mathrm{g,a}}(\omega) = \partial[\omega\epsilon_{\mathrm{a,R}}(\omega)]/\partial\omega$ is called the group permittivity of the active region. In (4), it is usually the threshold gain $g_{\mathrm{th},l}$ that is calculated from the quality factor Q_l and energy confinement factor $\Gamma_{\mathrm{E},l}$. While Q_l can be obtained from various numerical schemes, $\Gamma_{\mathrm{E},l}$ is often estimated in an indefinite manner from field integrations and leads to the uncertainty in $g_{\mathrm{th},l}$. Alternatively, we calculate $\Gamma_{\mathrm{E},l}$ from well-defined Q_l and $g_{\mathrm{th},l}$. The result can reveal what is missing in the conventional confinement factor calculated from field integrations, and the information might be useful for other computation schemes.

We utilize the formulation developed in [17] and outline the necessary information to obtain the confinement factor. The electric-field profile $\mathbf{f}_l(\mathbf{r},\omega)$ of mode l at a *real* frequency ω is the solution of the following generalized eigenvalue problem:

$$\nabla\times\nabla\times\mathbf{f}_l(\mathbf{r},\omega) - \left(\frac{\omega}{c}\right)^2 \bar{\bar{\epsilon}}_{\mathrm{r}}(\mathbf{r},\omega)\mathbf{f}_l(\mathbf{r},\omega)$$
$$= i\omega\mu_0\mathbf{j}_{\mathrm{s},l}(\mathbf{r},\omega) = \left(\frac{\omega}{c}\right)^2 \Delta\epsilon_{\mathrm{r},l}(\omega)U(\mathbf{r})\mathbf{f}_l(\mathbf{r},\omega) \tag{6a}$$

where $\bar{\bar{\epsilon}}_{\mathrm{r}}(\mathbf{r},\omega)$ is the relative permittivity tensor; $\Delta\epsilon_{\mathrm{r},l}(\omega)$ is the relative permittivity variation which makes mode l self-oscillating at frequency ω; $U(\mathbf{r})$ is the indicator function which equals unity in the active region but vanishes elsewhere; $\mathbf{j}_{\mathrm{s},l}(\mathbf{r},\omega) = -i\omega\epsilon_0\Delta\epsilon_{\mathrm{r},l}(\omega)U(\mathbf{r})\mathbf{f}_l(\mathbf{r},\omega)$ is the equivalent source current density; ϵ_0 and μ_0 are vacuum permittivity and permeability, respectively; and c is the speed of light in vacuum. For convenience, we define $\bar{\bar{\epsilon}}_{\mathrm{r,R}}(\mathbf{r},\omega) \equiv \mathrm{Re}[\bar{\bar{\epsilon}}_{\mathrm{r}}(\mathbf{r},\omega)]$, $\bar{\bar{\epsilon}}_{\mathrm{r,I}}(\mathbf{r},\omega) \equiv \mathrm{Im}[\bar{\bar{\epsilon}}_{\mathrm{r}}(\mathbf{r},\omega)]$, $\Delta\epsilon_{\mathrm{r},l,\mathrm{R}}(\omega) \equiv \mathrm{Re}[\Delta\epsilon_{\mathrm{r},l}(\omega)]$, and $\Delta\epsilon_{\mathrm{r},l,\mathrm{I}}(\omega) \equiv \mathrm{Im}[\Delta\epsilon_{\mathrm{r},l}(\omega)]$. Once $\mathbf{f}_l(\mathbf{r},\omega)$ is obtained, the corresponding magnetic-field profile is calculated from Faraday's law:

$$\mathbf{g}_l(\mathbf{r},\omega) = \frac{1}{i\omega\mu_0}\nabla\times\mathbf{f}_l(\mathbf{r},\omega). \tag{6b}$$

The permittivity variation $\Delta\epsilon_{\mathrm{r},l}(\omega)$ contains the spectral information of mode l. The resonance frequency ω_l is the one at which the magnitude $|\omega\Delta\epsilon_{\mathrm{r},l}(\omega)|$ is the minimum. The quality factor Q_l is obtained from the white-source condition of $\mathbf{j}_{\mathrm{s},l}(\mathbf{r},\omega)$ [17] and can be expressed as

$$Q_l = \frac{i}{2\Delta\epsilon_{\mathrm{r},l}(\omega_l)} \left.\frac{\partial[\omega\Delta\epsilon_{\mathrm{r},l}(\omega)]}{\partial\omega}\right|_{\omega=\omega_l}. \tag{7}$$

For a homogeneous and isotopic active region with the relative permittivity $\epsilon_{\rm a}(\omega)$ ($\epsilon_{\rm a,R}(\omega) \equiv {\rm Re}[\epsilon_{\rm a}(\omega)]$ and $\epsilon_{\rm a,I}(\omega) \equiv {\rm Im}[\epsilon_{\rm a}(\omega)]$), the threshold gain $g_{{\rm th},l}$ is obtained from the permittivity variation $\Delta\epsilon_{{\rm r},l}(\omega_l)$ at resonance with the cold-cavity condition [but the contribution from interstate transitions is excluded from $\epsilon_{\rm a}(\omega)$]:

$$g_{{\rm th},l} = -2\left(\frac{\omega_l}{c}\right){\rm Im}\left[\sqrt{\epsilon_{\rm a}(\omega_l)+\Delta\epsilon_{{\rm r},l}(\omega_l)}-\sqrt{\epsilon_{\rm a}(\omega_l)}\right]$$
$$\approx -\left(\frac{\omega_l}{c}\right)\frac{\Delta\epsilon_{{\rm r},l,{\rm I}}(\omega_l)}{\sqrt{\epsilon_{\rm a,R}(\omega_l)}} \quad (8)$$

where we have assumed that a proper amount of $\Delta\epsilon_{{\rm r},l}(\omega_l)$ is added into the active region, and $|\Delta\epsilon_{{\rm r},l,{\rm R}}(\omega_l)|$, $|\Delta\epsilon_{{\rm r},l,{\rm I}}(\omega_l)|$, and $|\epsilon_{\rm a,I}(\omega_l)|$ are much smaller than $\epsilon_{\rm a,R}(\omega_l)$. Note that the magnitude $|\Delta\epsilon_{{\rm r},l,{\rm I}}(\omega_l)|$ reflects how well the mode overlaps with the active region and how lossy the cavity is. The smaller magnitude indicates that the gain-field overlap is better, or the cavity becomes less lossy.

After substituting (5a), (5b), and (8) into (4), the inverse of the energy confinement factor is expressed as

$$\frac{1}{\Gamma_{{\rm E},l}} \approx -\frac{2Q_l\Delta\epsilon_{{\rm r},l,{\rm I}}(\omega_l)}{\epsilon_{\rm g,a}(\omega_l)+\epsilon_{\rm a,R}(\omega_l)}. \quad (9)$$

We note that $\Delta\epsilon_{{\rm r},l,{\rm I}}(\omega_l)$ is always negative so $\Gamma_{{\rm E},l}$ is a positive quantity. The relative permittivity $\epsilon_{\rm g,a}(\omega_l)$ and group permittivity $\epsilon_{\rm a,R}(\omega_l)$ in (9) are known in advance. Both the quality factor Q_l [see (7)] and imaginary part $\Delta\epsilon_{{\rm r},l,{\rm I}}(\omega_l)$ can be obtained with the knowledge of the eigenvalue $\Delta\epsilon_{{\rm r},l}(\omega)$, and the direct substitution of them into (9) leads to a well-defined energy confinement factor, which must be manifestly invariant to the integration region if this quantity should be numerically calculated with any field integrations. At this stage, it is unclear how the indefiniteness of the confinement factor from arbitrary integration regions could come into play. To clarify this point, we need a field representation for the energy confinement factor in (9).

III. Field Representation of Confinement Factor

The computation domain of a generic laser cavity is shown in Fig. 1. The integration region Ω contains the active region $\Omega_{\rm a}$. The surfaces of Ω and $\Omega_{\rm a}$ are denoted as S and $S_{\rm a}$, respectively. For simplicity, we consider an active region filled with the homogeneous and isotropic gain medium. Other parts of the cavity could be anisotropic.

We first write the quality factor Q_l in terms of various field integrals. From (7), Q_l is related to the frequency derivative of $\omega\Delta\epsilon_{{\rm r},l}(\omega)$ at ω_l, and therefore the frequency derivatives of fields are required. We define two analogous fields $\mathbf{p}_l(\mathbf{r})$ and $\mathbf{q}_l(\mathbf{r})$ from $\mathbf{f}_l(\mathbf{r},\omega)$ and $\mathbf{g}_l(\mathbf{r},\omega)$ as follows:

$$\mathbf{p}_l(\mathbf{r}) \equiv \omega_l\frac{\partial\mathbf{f}_l(\mathbf{r},\omega)}{\partial\omega}\bigg|_{\omega=\omega_l} \quad (10a)$$

$$\mathbf{q}_l(\mathbf{r}) \equiv \frac{1}{i\omega_l\mu_0}\nabla\times\mathbf{p}_l(\mathbf{r}) = \frac{\partial[\omega\mathbf{g}_l(\mathbf{r},\omega)]}{\partial\omega}\bigg|_{\omega=\omega_l}. \quad (10b)$$

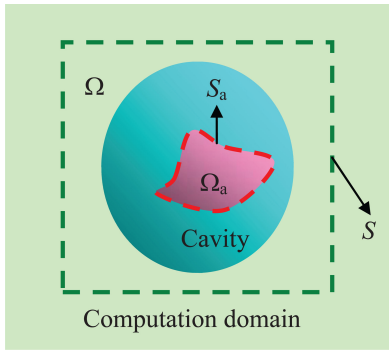

Fig. 1. Computation domain of a cavity structure. The integration region Ω contains the active region $\Omega_{\rm a}$. The surfaces of Ω and $\Omega_{\rm a}$ are denoted as S and $S_{\rm a}$, respectively.

We then take the frequency derivative $\omega[\partial/\partial\omega]$ at two sides of (6a), set $\omega=\omega_l$, and utilize the expression of Q_l in (7). In this way, the wave equation for $\mathbf{p}_l(\mathbf{r})$ is written as

$$\nabla\times\nabla\times\mathbf{p}_l(\mathbf{r}) - \left(\frac{\omega_l}{c}\right)^2\left[\bar{\bar{\epsilon}}_{\rm r}(\mathbf{r},\omega_l)+\Delta\epsilon_{{\rm r},l}(\omega_l)U(\mathbf{r})\,\bar{\bar{I}}\right]\mathbf{p}_l(\mathbf{r})$$
$$= \left(\frac{\omega_l}{c}\right)^2\left[\bar{\bar{\epsilon}}^{\rm (c)}_{\rm g}(\mathbf{r},\omega_l)+\bar{\bar{\epsilon}}_{\rm r}(\mathbf{r},\omega_l)\right.$$
$$\left.+(1-2iQ_l)\Delta\epsilon_{{\rm r},l}(\omega_l)U(\mathbf{r})\,\bar{\bar{I}}\right]\mathbf{f}_l(\mathbf{r},\omega_l) \quad (11)$$

where $\bar{\bar{\epsilon}}^{\rm (c)}_{\rm g}(\mathbf{r},\omega) \equiv \partial[\omega\,\bar{\bar{\epsilon}}_{\rm r}(\mathbf{r},\omega)]/\partial\omega$ is called the complex group permittivity tensor. Next, we dot-product both sides of (11) with the field $\mathbf{f}_l^*(\mathbf{r},\omega_l)$ and integrate over the integration region Ω. With a similar procedure to the integration by parts and applications of divergence theorem, we obtain the following integral identity:

$$i\omega_l\mu_0\oint_S {\rm d}\mathbf{a}\cdot[\mathbf{q}_l(\mathbf{r})\times\mathbf{f}_l^*(\mathbf{r},\omega_l)-\mathbf{p}_l(\mathbf{r})\times\mathbf{g}_l^*(\mathbf{r},\omega_l)]$$
$$+\int_\Omega {\rm d}\mathbf{r}\left\{\nabla\times\nabla\times\mathbf{f}_l(\mathbf{r},\omega_l)\right.$$
$$\left.-\left[\bar{\bar{\epsilon}}_{\rm r}(\mathbf{r},\omega_l)+\Delta\epsilon_{{\rm r},l}(\omega_l)U(\mathbf{r})\,\bar{\bar{I}}\right]\mathbf{f}_l(\mathbf{r},\omega_l)\right\}^*\cdot\mathbf{p}_l(\mathbf{r})$$
$$-2i\left(\frac{\omega_l}{c}\right)^2\int_\Omega {\rm d}\mathbf{r}\mathbf{f}_l^*(\mathbf{r},\omega_l)\cdot\bar{\bar{\epsilon}}_{{\rm r},{\rm I}}(\mathbf{r},\omega_l)\mathbf{p}_l(\mathbf{r})$$
$$-2i\left(\frac{\omega_l}{c}\right)^2\Delta\epsilon_{{\rm r},l,{\rm I}}(\omega_l)\int_{\Omega_{\rm a}}{\rm d}\mathbf{r}\mathbf{f}_l^*(\mathbf{r},\omega_l)\cdot\mathbf{p}_l(\mathbf{r})$$
$$=\left(\frac{\omega_l}{c}\right)^2\int_\Omega {\rm d}\mathbf{r}\mathbf{f}_l^*(\mathbf{r},\omega_l)\cdot\left[\bar{\bar{\epsilon}}^{\rm (c)}_{\rm g}(\mathbf{r},\omega_l)+\bar{\bar{\epsilon}}_{\rm r}(\mathbf{r},\omega_l)\right]\mathbf{f}_l(\mathbf{r},\omega_l)$$
$$+(1-2iQ_l)\left(\frac{\omega_l}{c}\right)^2\Delta\epsilon_{{\rm r},l}(\omega_l)\int_{\Omega_{\rm a}}{\rm d}\mathbf{r}|\mathbf{f}_l(\mathbf{r},\omega_l)|^2 \quad (12)$$

where we have utilized the fact that $\bar{\bar{\epsilon}}_{\rm r}(\mathbf{r},\omega)$ on the third line is a symmetric tensor in reciprocal environments. The volume integral on the second and third lines of (12) is zero due to the wave equation of $\mathbf{f}_l(\mathbf{r},\omega_l)$ in (6a). Taking the real parts at both sides of (12), we then express Q_l in terms of various integrals

of fields as

$$Q_l = -\frac{\int_\Omega \mathrm{d}\mathbf{r}\mathbf{f}_l^*(\mathbf{r},\omega_l)\cdot\left[\overline{\overline{\epsilon}}_{\mathrm{g}}(\mathbf{r},\omega_l)+\overline{\overline{\epsilon}}_{\mathrm{r,R}}(\mathbf{r},\omega_l)\right]\mathbf{f}_l(\mathbf{r},\omega_l)}{2\Delta\epsilon_{\mathrm{r},l,\mathrm{I}}(\omega_l)\int_{\Omega_\mathrm{a}}\mathrm{d}\mathbf{r}|\mathbf{f}_l(\mathbf{r},\omega_l)|^2}$$
$$-\frac{\Delta\epsilon_{\mathrm{r},l,\mathrm{R}}(\omega_l)}{2\Delta\epsilon_{\mathrm{r},l,\mathrm{I}}(\omega_l)}+\frac{\int_\Omega \mathrm{d}\mathbf{r}\mathrm{Im}\left[\mathbf{f}_l^*(\mathbf{r},\omega_l)\cdot\overline{\overline{\epsilon}}_{\mathrm{r,I}}(\mathbf{r},\omega_l)\mathbf{p}_l(\mathbf{r})\right]}{\Delta\epsilon_{\mathrm{r},l,\mathrm{I}}(\omega_l)\int_{\Omega_\mathrm{a}}\mathrm{d}\mathbf{r}|\mathbf{f}_l(\mathbf{r},\omega_l)|^2}$$
$$+\frac{\int_{\Omega_\mathrm{a}}\mathrm{d}\mathbf{r}\mathrm{Im}\left[\mathbf{f}_l^*(\mathbf{r},\omega_l)\cdot\mathbf{p}_l(\mathbf{r})\right]}{\int_{\Omega_\mathrm{a}}\mathrm{d}\mathbf{r}|\mathbf{f}_l(\mathbf{r},\omega_l)|^2}$$
$$-\frac{\frac{1}{\omega_l\epsilon_0}\oint_S \mathrm{d}\mathbf{a}\cdot\mathrm{Im}[\mathbf{q}_l(\mathbf{r})\times\mathbf{f}_l^*(\mathbf{r},\omega_l)-\mathbf{p}_l(\mathbf{r})\times\mathbf{g}_l^*(\mathbf{r},\omega_l)]}{2\Delta\epsilon_{\mathrm{r},l,\mathrm{I}}(\omega_l)\int_{\Omega_\mathrm{a}}\mathrm{d}\mathbf{r}|\mathbf{f}_l(\mathbf{r},\omega_l)|^2} \tag{13}$$

where $\overline{\overline{\epsilon}}_{\mathrm{g}}(\mathbf{r},\omega)=\mathrm{Re}[\overline{\overline{\epsilon}}_{\mathrm{g}}^{(\mathrm{c})}(\mathbf{r},\omega)]$ ($\overline{\overline{\epsilon}}_{\mathrm{g}}(\mathbf{r},\omega)$ will be referred as the group permittivity tensor). After the substitution of (13) into (9), the field representation of $\Gamma_{\mathrm{E},l}$ is obtained as follows:

$$\frac{1}{\Gamma_{\mathrm{E},l}}\approx\frac{\int_\Omega \mathrm{d}\mathbf{r}\mathbf{f}_l^*(\mathbf{r},\omega_l)\cdot\frac{\epsilon_0}{4}\left[\overline{\overline{\epsilon}}_{\mathrm{g}}(\mathbf{r},\omega_l)+\overline{\overline{\epsilon}}_{\mathrm{r,R}}(\mathbf{r},\omega_l)\right]\mathbf{f}_l(\mathbf{r},\omega_l)}{\int_{\Omega_\mathrm{a}}\mathrm{d}\mathbf{r}\frac{\epsilon_0}{4}[\epsilon_{\mathrm{g,a}}(\omega_l)+\epsilon_{\mathrm{a,R}}(\omega_l)]|\mathbf{f}_l(\mathbf{r},\omega_l)|^2}$$
$$+\frac{\Delta\epsilon_{\mathrm{r},l,\mathrm{R}}(\omega_l)}{[\epsilon_{\mathrm{g,a}}(\omega_l)+\epsilon_{\mathrm{a,R}}(\omega_l)]}$$
$$-\frac{\int_\Omega \mathrm{d}\mathbf{r}\frac{\epsilon_0}{2}\mathrm{Im}\left[\mathbf{f}_l^*(\mathbf{r},\omega_l)\cdot\overline{\overline{\epsilon}}_{\mathrm{r,I}}(\mathbf{r},\omega_l)\mathbf{p}_l(\mathbf{r})\right]}{\int_{\Omega_\mathrm{a}}\mathrm{d}\mathbf{r}\frac{\epsilon_0}{4}[\epsilon_{\mathrm{g,a}}(\omega_l)+\epsilon_{\mathrm{a,R}}(\omega_l)]|\mathbf{f}_l(\mathbf{r},\omega_l)|^2}$$
$$-\frac{\Delta\epsilon_{\mathrm{r},l,\mathrm{I}}(\omega_l)\int_{\Omega_\mathrm{a}}\mathrm{d}\mathbf{r}\frac{\epsilon_0}{2}\mathrm{Im}\left[\mathbf{f}_l^*(\mathbf{r},\omega_l)\cdot\mathbf{p}_l(\mathbf{r})\right]}{\int_{\Omega_\mathrm{a}}\mathrm{d}\mathbf{r}\frac{\epsilon_0}{4}[\epsilon_{\mathrm{g,a}}(\omega_l)+\epsilon_{\mathrm{a,R}}(\omega_l)]|\mathbf{f}_l(\mathbf{r},\omega_l)|^2}$$
$$+\frac{\frac{1}{4\omega_l}\oint_S \mathrm{d}\mathbf{a}\cdot\mathrm{Im}[\mathbf{q}_l(\mathbf{r})\times\mathbf{f}_l^*(\mathbf{r},\omega_l)-\mathbf{p}_l(\mathbf{r})\times\mathbf{g}_l^*(\mathbf{r},\omega_l)]}{\int_{\Omega_\mathrm{a}}\mathrm{d}\mathbf{r}\frac{\epsilon_0}{4}[\epsilon_{\mathrm{g,a}}(\omega_l)+\epsilon_{\mathrm{a,R}}(\omega_l)]|\mathbf{f}_l(\mathbf{r},\omega_l)|^2}. \tag{14}$$

The first line on the right-hand side (RHS) of (14) is the inverse of the conventional energy confinement factor $\Gamma_{\mathrm{E},l}^{(\mathrm{old})}(\Omega)$:

$$\frac{1}{\Gamma_{\mathrm{E},l}^{(\mathrm{old})}(\Omega)}$$
$$\equiv\frac{\int_\Omega \mathrm{d}\mathbf{r}\mathbf{f}_l^*(\mathbf{r},\omega_l)\cdot\frac{\epsilon_0}{4}\left[\overline{\overline{\epsilon}}_{\mathrm{g}}(\mathbf{r},\omega_l)+\overline{\overline{\epsilon}}_{\mathrm{r,R}}(\mathbf{r},\omega_l)\right]\mathbf{f}_l(\mathbf{r},\omega_l)}{\int_{\Omega_\mathrm{a}}\mathrm{d}\mathbf{r}\frac{\epsilon_0}{4}[\epsilon_{\mathrm{g,a}}(\omega_l)+\epsilon_{\mathrm{a,R}}(\omega_l)]|\mathbf{f}_l(\mathbf{r},\omega_l)|^2}. \tag{15}$$

In addition to this conventional term, other counter terms, which maintain the invariance of $\Gamma_{\mathrm{E},l}$ to an arbitrary integration region Ω, are also present. Since Ω can be any regions containing Ω_a, the uncertainty on the first line on the RHS of (14) has to be removed by the presence of other terms. Among these counter terms, the one proportional to the surface integral on the last line of (14) is of particular importance because it is this term that eliminates the indefiniteness brought by $\Gamma_{\mathrm{E},l}^{(\mathrm{old})}(\Omega)$ in the lossless free space, namely, the exclusion of the irrelevant contribution from the far field.

Still, specific constraints need to be imposed on the fields $\mathbf{p}_l(\mathbf{r})$ and $\mathbf{q}_l(\mathbf{r})$ because their solutions are not unique. This fact can be observed from (11). The operator acting on $\mathbf{p}_l(\mathbf{r})$ on the left-hand side (LHS) of (11) has the homogeneous solution of $\mathbf{f}_l(\mathbf{r},\omega_l)$. The addition of any terms proportional to $\mathbf{f}_l(\mathbf{r},\omega_l)$ to the particular solution of $\mathbf{p}_l(\mathbf{r})$ remains a solution to the wave equation in (11). This additional degree of freedom can be utilized to simplify the field representation of $\Gamma_{\mathrm{E},l}$ if one would calculate it from (14) rather than (9). The detail is presented in Appendix A for interested readers.

The invariance of $\Gamma_{\mathrm{E},l}$ can be inferred from the RHS of (9) because the quantities there are all well defined. However, this property is less obvious from the field representation in (14). As a consistency check, a proof for the invariance of the field representation in (14) to the integration regions containing Ω_a is provided in Appendix B based on the generalized Poynting theorem. The proof also makes the origin of counterterm integrals clearer.

IV. Modal Volumes

The self-consistent energy confinement factor in (9) can be utilized to define modal volumes of cavity modes invariant to integration regions. When $\Gamma_{\mathrm{E},l}$ is adopted in the laser rate equations [8], the effective modal volume $V_{\mathrm{eff},l}$ used in photon-density calculations is written as

$$V_{\mathrm{eff},l}\equiv\frac{V_\mathrm{a}}{\Gamma_{\mathrm{E},l}}=\frac{V_\mathrm{a}}{\Gamma_{\mathrm{E},l}^{(\mathrm{old})}(\Omega)}+[\text{counter terms}] \tag{16a}$$

where V_a is the volume of the active region. On the other hand, for the cavity QED and Purcell effect, another modal volume $V_{\mathrm{QM},l}$ of the cavity mode is often preferred (slightly modified from the expression for nondispersive cavities [18]):

$$V_{\mathrm{QM},l}\equiv\frac{\frac{1}{\Gamma_{\mathrm{E},l}}\int_{\Omega_\mathrm{a}}\mathrm{d}\mathbf{r}\frac{\epsilon_0}{4}[\epsilon_{\mathrm{g,a}}(\omega_l)+\epsilon_{\mathrm{a,R}}(\omega_l)]|\mathbf{f}_l(\mathbf{r},\omega_l)|^2}{\mathbf{f}_l^*(\mathbf{r}_\mathrm{p},\omega_l)\cdot\frac{\epsilon_0}{4}\left[\overline{\overline{\epsilon}}_{\mathrm{g}}(\mathbf{r}_\mathrm{p},\omega_l)+\overline{\overline{\epsilon}}_{\mathrm{r,R}}(\mathbf{r}_\mathrm{p},\omega_l)\right]\mathbf{f}_l(\mathbf{r}_\mathrm{p},\omega_l)}$$
$$=\frac{\int_\Omega \mathrm{d}\mathbf{r}\mathbf{f}_l^*(\mathbf{r},\omega_l)\cdot\frac{\epsilon_0}{4}\left[\overline{\overline{\epsilon}}_{\mathrm{g}}(\mathbf{r},\omega_l)+\overline{\overline{\epsilon}}_{\mathrm{r,R}}(\mathbf{r},\omega_l)\right]\mathbf{f}_l(\mathbf{r},\omega_l)}{\mathbf{f}_l^*(\mathbf{r}_\mathrm{p},\omega_l)\cdot\frac{\epsilon_0}{4}\left[\overline{\overline{\epsilon}}_{\mathrm{g}}(\mathbf{r}_\mathrm{p},\omega_l)+\overline{\overline{\epsilon}}_{\mathrm{r,R}}(\mathbf{r}_\mathrm{p},\omega_l)\right]\mathbf{f}_l(\mathbf{r}_\mathrm{p},\omega_l)}$$
$$+[\text{counter terms}] \tag{16b}$$

where $\mathbf{r}_\mathrm{p}$ is the position at which $|\mathbf{f}_l(\mathbf{r},\omega_l)|^2$ is the peak value. The two modal volumes $V_{\mathrm{eff},l}$ and $V_{\mathrm{QM},l}$ in (16a) and (16b), respectively, are physical because they are calculated from finite and well-defined quantities rather than their conventional counterparts [the expressions other than the counter terms in (16a) and (16b)] . The effect of far field has been removed from these expressions by the counter terms.

V. Application to WGMs in Dielectric Sphere

We apply this self-consistent method to WGMs of a lossless dielectric microsphere in Fig. 2, and show how the indefiniteness of the integration region comes into play. The sphere has a radius R of 5 μm. Outside the sphere is the free space of vacuum (unity relative permittivity). The active region Ω_a is chosen as the whole region inside the sphere, and its permittivity ϵ_a is independent of the frequency and set to 2.25.

For each angular momentum (AM) mode number $L\in\mathbb{Z}^+$, we consider the radially fundamental and second-order WGMs (radial mode number $N=1,2$) consisting of the profiles with

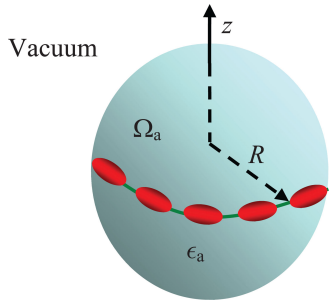

Fig. 2. Dielectric spherical cavity (radius $R = 5\,\mu$m) which supports WGMs. Outside the sphere is the free space of vacuum with the unity relative permittivity while the inner is the dielectric with a relative permittivity $\epsilon_a = 2.25$.

the largest magnitude of AM in the z direction (azimuthal mode number $M = \pm L$). In addition to these mode numbers, the modes can be further classified as radially transverse magnetic (TM_r) or radially transverse electric (TE_r). Thus, the mode label l contains a set of indices $l = (\tilde{l}, |M|, \beta) = (\tilde{l}, L, \beta)$, where $\tilde{l} = (\alpha, N, L)$; $\alpha = 1(0)$ represents TM_r (TE_r); and $\beta = \pm 1$ indicates two possibilities for the azimuthal dependence except for $M = 0$. The mode profiles $\mathbf{f}_l(\mathbf{r}, \omega)$ of the WGMs are written as

$$\bullet \mathrm{TM_r}[\tilde{l} = (\alpha, N, L) = (1, N, L)]$$

$$\mathbf{f}_l(\mathbf{r}, \omega) = \hat{r} f_{\tilde{l},\parallel}(r, \omega) \frac{[Y_{LL}(\theta, \phi) + \beta Y^*_{LL}(\theta, \phi)]}{\sqrt{2} i^{(1-\beta)/2}} + \hat{\theta} f_{\tilde{l},\perp}(r, \omega) \frac{\partial}{\partial \theta} \frac{[Y_{LL}(\theta, \phi) + \beta Y^*_{LL}(\theta, \phi)]}{\sqrt{2} i^{(1-\beta)/2} L(L+1)} + \hat{\phi} f_{\tilde{l},\perp}(r, \omega) \frac{i[Y_{LL}(\theta, \phi) - \beta Y^*_{LL}(\theta, \phi)]}{\sqrt{2} i^{(1-\beta)/2} (L+1) \sin\theta} \quad (17a)$$

$$\bullet \mathrm{TE_r}[\tilde{l} = (\alpha, N, L) = (0, N, L)]$$

$$\mathbf{f}_l(\mathbf{r}, \omega) = \hat{\theta} f_{\tilde{l},\perp}(r, \omega) \frac{\partial}{\partial \theta} \frac{[Y_{LL}(\theta, \phi) + \beta Y^*_{LL}(\theta, \phi)]}{\sqrt{2} i^{(1-\beta)/2} L(L+1)} + \hat{\phi} f_{\tilde{l},\perp}(r, \omega) \frac{i[Y_{LL}(\theta, \phi) - \beta Y^*_{LL}(\theta, \phi)]}{\sqrt{2} i^{(1-\beta)/2} (L+1) \sin\theta} \quad (17b)$$

where $f_{\tilde{l},\parallel}(r, \omega)$ [$f_{\tilde{l},\perp}(r, \omega)$] is the field amplitude parallel (perpendicular) to the radial direction; and $Y_{LL}(\theta, \phi)$ is the spherical harmonic with $M = L$. Inside (outside) the sphere, the field amplitudes $f_{\tilde{l},\parallel}(r, \omega)$ and $f_{\tilde{l},\perp}(r, \omega)$ are closely related to the spherical Bessel (Hankel) function j_L [$h_L^{(1)}$] of the first kind. After matching the boundary conditions of the fields at $r = R$, we obtain the following transcendental equation for the TM_r ($\alpha = 1$) and TE_r ($\alpha = 0$) WGMs:

$$[\epsilon_a + \Delta\epsilon_{r,l}(\omega)]^{(1-2\alpha)/2} \left\{ \frac{1}{x j_L(x)} \frac{\mathrm{d}[x j_L(x)]}{\mathrm{d}x} \right\}_{x = k_a R} = \left\{ \frac{1}{x h_L^{(1)}(x)} \frac{\mathrm{d}[x h_L^{(1)}(x)]}{\mathrm{d}x} \right\}_{x = k_0 R} \quad (18)$$

where $k_0 = \omega/c$ and $k_a = k_0 \sqrt{\epsilon_a + \Delta\epsilon_{r,l}(\omega)}$ are the propagation constants in the vacuum and sphere, respectively. The permittivity variation $\Delta\epsilon_{r,l}(\omega)$ is numerically calculated for a range of frequency ω. The parameters ω_l, Q_l, and $\Delta\epsilon_{r,l,I}(\omega_l)$ are then obtained from the spectral information of $\Delta\epsilon_{r,l}(\omega)$, as described in Section II.

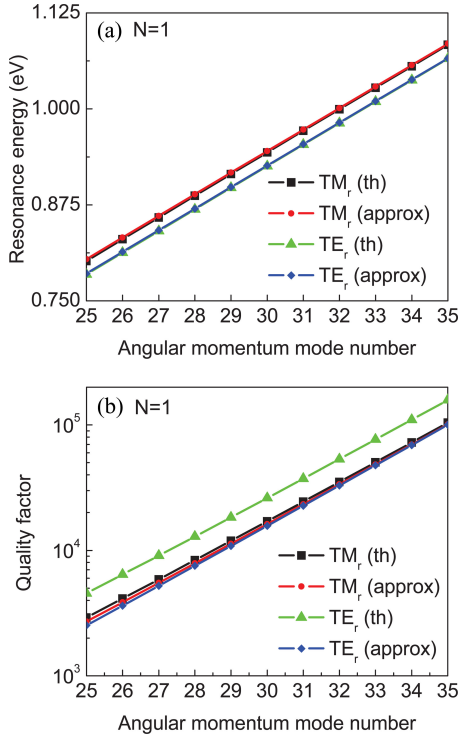

Fig. 3. (a) Comparison between the theoretical resonance energies $\hbar\omega_l$ and corresponding analytical approximations [23] for the fundamental TM_r and TE_r WGMs. The theoretical and analytical results match well. (b) Comparison between the theoretical quality factors Q_l and corresponding analytical approximations [24] for the same modes. There are significant deviations for the TE_r WGMs.

Fig. 3(a) shows the comparison between the theoretical resonance energies $\hbar\omega_l$ and analytical approximations based on the asymptotic expansions of spherical Bessel functions [23] for the radially fundamental TM_r and TE_r WGMs (the corresponding wavelengths roughly cover the range of 1.1–1.55 μm). The theoretical results agree well with those calculated from the analytical expressions. On the other hand, in Fig. 3(b), the theoretical quality factors Q_l calculated from (7) exhibit deviations from analytical approximations based on the asymptotic expansions [24]. The deviations are more significant for the TE_r WGMs and can be as large as 45%. The same observations had been reported in calculations based on the complex-ω method [25], indicating that the asymptotic expansion is accurate in the order of magnitude rather than the absolute value for Q factors.

In fact, the resonance energies and Q factors obtained from the spectral information of $\Delta\epsilon_{r,l}(\omega)$ almost coincide with those from the complex-ω method, but the divergent far field is absent in the former. We also believe that the Q factors calculated from the current scheme are more physical than those estimated from the asymptotic expansions because they lead to sensible magnitudes of the energy confinement factors and modal volumes. The energy confinement factors $\Gamma_{E,l}$ in Fig. 4(a) are calculated

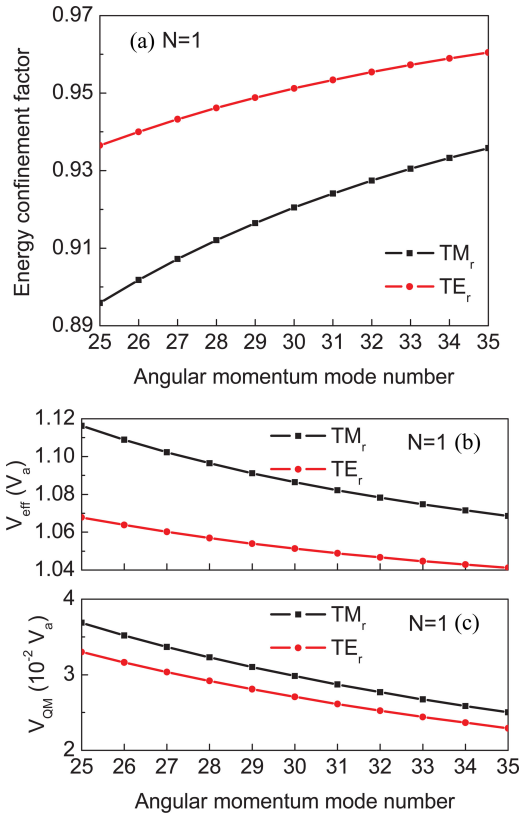

Fig. 4. (a) Energy confinement factors $\Gamma_{\mathrm{E},l}$ of WGMs with different Ls. The magnitudes of $\Gamma_{\mathrm{E},l}$s are lower than unity. (b) Modal volumes $V_{\mathrm{eff},l}$ of the same modes. Reflecting the fact that $\Gamma_{\mathrm{E},l} \leq 1$, $V_{\mathrm{eff},l}$s are larger than V_{a}. (c) Modal volumes $V_{\mathrm{QM},l}$, which are small fractions of V_{a} due to the localization of fundamental WGMs near the surface of the sphere.

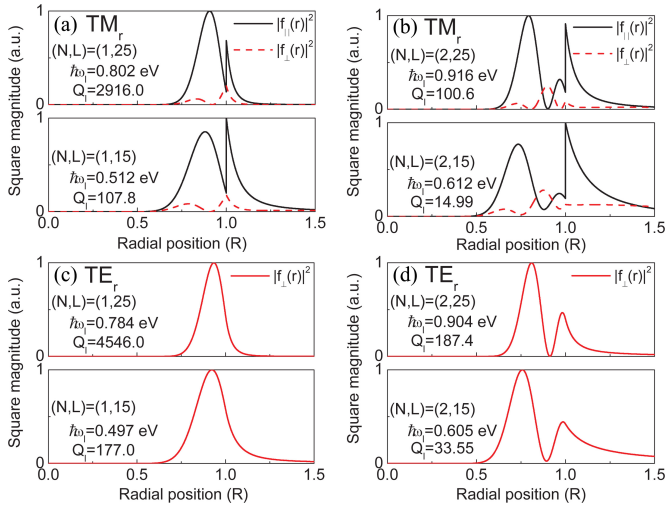

Fig. 5. Square magnitudes of the mode profiles for the radially (a) fundamental ($N = 1$) TM$_r$, (b) second-order ($N = 2$) TM$_r$, (c) fundamental ($N = 1$) TE$_r$, and (d) second-order ($N = 2$) TE$_r$ WGMs. The upper and lower graphs in each figure represent the profiles of WGMs with $L = 25$ and $L = 15$, respectively. The corresponding resonance energies and Q factors are marked inside the graphs. In general, Q factors of the TE$_r$ WGMs are higher. The same trend applies to WGMs with the larger L or smaller N.

from Q_l in (7) and $\Delta\epsilon_{\mathrm{r},l,\mathrm{I}}(\omega_l)$ [see (9)] and exhibit magnitudes less than unity. This behavior reflects the imperfect overlaps between the WGMs and the active region Ω_{a}. If the analytical approximation of the Q factor based on the asymptotic expansions of spherical Bessel functions were used, $\Gamma_{\mathrm{E},l}$ of the TE$_r$ WGMs would be well above unity—unreasonable overlaps between the mode profiles and gain medium. While the fundamental TE$_r$ WGMs are better confined than the TM$_r$ counterparts, both types of modes exhibit increasing $\Gamma_{\mathrm{E},l}$ as the AM mode number L becomes larger, indicating the less leakage into the free space and better field-gain overlaps. In Fig. 4(a) and (b), we show the modal volumes $V_{\mathrm{eff},l}$ and $V_{\mathrm{QM},l}$ [(16a) and (16b)], respectively, in the unit of $V_{\mathrm{a}} = 4\pi R^3/3$. The modal volumes $V_{\mathrm{eff},l}$ of the WGMs are larger than V_{a} and decrease with the AM mode number L, reflecting the trend of $\Gamma_{\mathrm{E},l}^{-1}$ in (16a). Contrary to $V_{\mathrm{eff},l}$s, the modal volumes $V_{\mathrm{QM},l}$ of these fundamental WGMs are small fractions of V_{a} because they are a measure of how well the modes are localized around the respective field peaks, which are located near the surface of the sphere. Analogous to the trend of $V_{\mathrm{eff},l}$s, $V_{\mathrm{QM},l}$s of various WGMs decrease with the AM mode number L due to the more enhanced confinement near the surface. In addition, the fundamental TE$_r$ WGMs are better localized than their TM$_r$ counterparts because discontinuities of the radial components $f_{\tilde{l},\parallel}(r,\omega_l)$ at $r = R$ bring about the more significant tails of the fields resident in the free space.

To see how the indefiniteness due to different choices of integration regions comes into play, we consider the mode profiles and energy confinement factors $\Gamma_{\mathrm{E},l}^{(\mathrm{old})}(\Omega)$ of the TM$_r$ and TE$_r$ WGMs with the AM mode number $L = 15, 25$ and radial mode number $N = 1, 2$ as a function of the integration region Ω. The region Ω is set to a ball concentric to the microsphere and has a radius R_{b} (integration boundary) larger than R. The square magnitudes ($|f_{\tilde{l},\parallel}(r,\omega_l)|^2$ and $|f_{\tilde{l},\perp}(r,\omega_l)|^2$) of the TM$_r$ mode profiles are shown in Fig. 5(a) ($N = 1$) and (b) ($N = 2$), and those of the TE$_r$ modes ($|f_{\tilde{l},\perp}(r,\omega_l)|^2$) are presented in Fig. 5(c) ($N = 1$) and (d) ($N = 2$). In each figure, the upper and lower graphs indicate the mode profiles for $L = 25$ and $L = 15$, respectively. The corresponding resonance photon energies and Q factors are also marked in the graphs. In general, the Q factors of the TE$_r$ WGMs are higher than those of the TM$_r$ counterparts, as reflected in the less conspicuous tails of the TE$_r$ modes extending into the free space. Similarly, the modes with the larger AM mode numbers L have the higher Q factors (the upper graph versus lower one in each figure) because the formers are better confined in the peripheral of the sphere and less leakier into the free space. On the other hand, the opposite trend takes place for modes with the higher radial mode number N [Fig. 5(a) versus (b); and Fig. 5(c) versus (d)]. For these modes, the more nodes (or more oscillatory behaviors) on the mode profiles along the radial direction indicate that the radial momentum is more significant. Photons coupled to these modes leave the cavity more easily, which results in the lower Q factors.

Corresponding to the profiles in Fig. 5, the conventional energy confinement factors $\Gamma_{\mathrm{E},l}^{(\mathrm{old})}(\Omega)$ of the WGMs as a function of the integration boundary near the sphere radius are shown in Fig. 6. In addition to $\Gamma_{\mathrm{E},l}^{(\mathrm{old})}(\Omega)$ calculated from the profiles in (17a) and (17b) and definite counterparts $\Gamma_{\mathrm{E},l}$, we also show $\Gamma_{\mathrm{E},l}^{(\mathrm{old})}(\Omega)$ obtained from the profiles based on the complex-ω

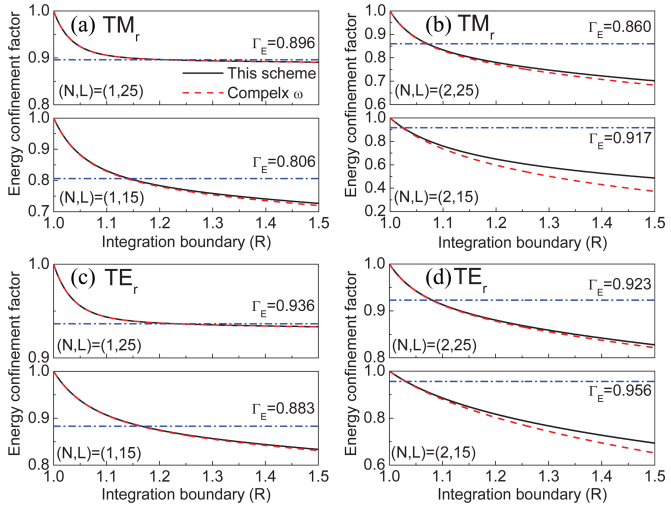

Fig. 6. Various energy confinement factors in the range of $R_b \gtrsim R$ for (a) TM$_r$ WGMs with $N = 1$, (b) TM$_r$ WGMs with $N = 2$, (c) TE$_r$ WGMs with $N = 1$, and (d) TE$_r$ WGMs with $N = 2$ (black solid: $\Gamma_{\mathrm{E},l}^{(\mathrm{old})}(\Omega)$ based on the current scheme; red dash: the counterpart based on the complex-ω method; and blue dash–dotted: $\Gamma_{\mathrm{E},l}$). For the high-Q WGMs in (a) and (c) $[(N, L) = (1, 25)]$, $\Gamma_{\mathrm{E},l}^{(\mathrm{old})}(\Omega)$s are close to $\Gamma_{\mathrm{E},l}$s in a considerable range. On the other hand, these ranges are narrower for other low-Q WGMs.

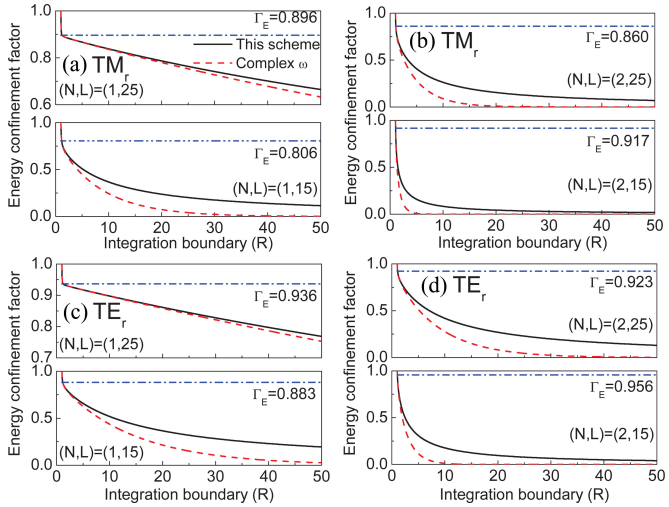

Fig. 7 Various energy confinement factors in the wider range of R_b for (a) TM$_r$ WGMs with $N = 1$, (b) TM$_r$ WGMs with $N = 2$, (c) TE$_r$ WGMs with $N = 1$, and (d) TE$_r$ WGMs with $N = 2$ (identical line styles to those in Fig. 6). All $\Gamma_{\mathrm{E},l}^{(\mathrm{old})}(\Omega)$s of the WGMs ultimately deviate from the respective $\Gamma_{\mathrm{E},l}$s in the large R_{b} limit. In addition, $\Gamma_{\mathrm{E},l}^{(\mathrm{old})}(\Omega)$s based on the complex-$\omega$ method decrease exponentially as R_b increases.

method. For $R_{\mathrm{b}} \gtrsim R$, the conventional energy confinement factors based on the current scheme and complex-ω method do not differ much since their near-field profiles resemble each other. We note that the differences on the field leakage lead to distinct behaviors of $\Gamma_{\mathrm{E},l}^{(\mathrm{old})}(\Omega)$ for these WGMs. From the upper graphs in Fig. 6(a) and (c), the conventional energy confinement factor $\Gamma_{\mathrm{E},l}^{(\mathrm{old})}(\Omega)$ of the TM$_r$ and TE$_r$ WGMs with $(N, L) = (1, 25)$ are close to their definite counterparts over a considerable range around $R_{\mathrm{b}} \approx 1.21R$ and $R_{\mathrm{b}} \approx 1.23R$, respectively. This characteristic is common to both radially fundamental TM$_r$ and TE$_r$ WGMs with large AM mode numbers L. Thus, it can be inferred that for modes with high radiative Q factors, $\Gamma_{\mathrm{E},l}^{(\mathrm{old})}(\Omega)$ obtained from field integrations should be close to $\Gamma_{\mathrm{E},l}$ if the integration region Ω is decently but not excessively large. On the other hand, for other modes with the much lower Q factors, the condition $\Gamma_{\mathrm{E},l}^{(\mathrm{old})}(\Omega) \approx \Gamma_{\mathrm{E},l}$ is valid in a much narrower range. Above a certain integration boundary, $\Gamma_{\mathrm{E},l}^{(\mathrm{old})}(\Omega)$ quickly drops below its definite counterpart $\Gamma_{\mathrm{E},l}$, indicating that $\Gamma_{\mathrm{E},l}^{(\mathrm{old})}(\Omega)$ is sensitive to the integration region Ω. The observation applies to resonance modes with low radiative Q factors in various cavity structures. This situation may take place in small lasers such as those made of nanocrystals [26]–[28] or those without sharp borders or feedback reflectors at which photons leave the cavity [29]. Care is required in the choice of integration region Ω when modeling these cavity structures. Also, the radiative Q factor and energy confinement factor $\Gamma_{\mathrm{E},l}$ are not always positive correlated. From the lower graphs in Fig. 6, both of the TM$_r$ and TE$_r$ WGMs with $(N, L) = (2, 15)$ have the larger $\Gamma_{\mathrm{E},l}$s than their counterparts with $(N, L) = (1, 15)$ do, but the corresponding Q factors behave the other way around. Comparing the profiles of TM$_r$ (TE$_r$) WGMs with $(N, L) = (1, 15)$ and $(N, L) = (2, 15)$ in the lower graphs of Fig. 5(a) and (b) [Fig. 5(c) and (d)], the higher order modes are distributed closer to the sphere center despite the more significant field tails into the free space. In fact, the higher $\Gamma_{\mathrm{E},l}$s of WGMs with $(N, L) = (2, 15)$ than those of the modes with $(N, L) = (1, 15)$ reflect the exclusion of far-field contributions from $\Gamma_{\mathrm{E},l}$ so that the fields inside/near the sphere play the more important role in lasing and modal volumes.

Although the valid integration range for high-Q WGMs is wider, the corresponding conventional energy confinement factors $\Gamma_{\mathrm{E},l}^{(\mathrm{old})}(\Omega)$ ultimately deviate from their definite counterparts $\Gamma_{\mathrm{E},l}$ and approach zero as the integration region extends to infinity. The behaviors of $\Gamma_{\mathrm{E},l}^{(\mathrm{old})}(\Omega)$s are shown in Fig. 7 for sufficiently large integration boundaries. For all $\Gamma_{\mathrm{E},l}^{(\mathrm{old})}(\Omega)$s in Fig. 7, the uncertainty due to the integration region Ω shows up as R_{b} becomes large, even though practical computations do not often reach this regime. From the comparison between $\Gamma_{\mathrm{E},l}^{(\mathrm{old})}(\Omega)$s of the high-$Q$ WGMs with $(N, L) = (1, 25)$ [upper graphs of Fig. 7(a) and (c)] and those of other low-Q modes, although the conventional energy confinement factors of high-Q modes do drop less rapidly than those of low-Q modes, this trend does not prevent $\Gamma_{\mathrm{E},l}^{(\mathrm{old})}(\Omega)$s of high-$Q$ modes from vanishing at the larger R_{b}. In addition, while for high-Q modes the dependences of $\Gamma_{\mathrm{E},l}^{(\mathrm{old})}(\Omega)$s on R_{b} using mode profiles from the current scheme and complex-ω method are similar [upper graphs of Fig. 7(a) and (c)], the counterparts of other low-Q modes behave distinctly. The conventional energy confinement factor based on the current scheme has an asymptotic dependence of R_{b}^{-1}, but that based on the complex-ω method decreases exponentially due to the divergent far field. These divergent far fields of lower-Q WGMs exhibit the more rapid exponential growth $\exp[\omega_l r/(2cQ_l)]$ toward the free space. Therefore, the applicable range of the integration boundary R_{b} of the conventional

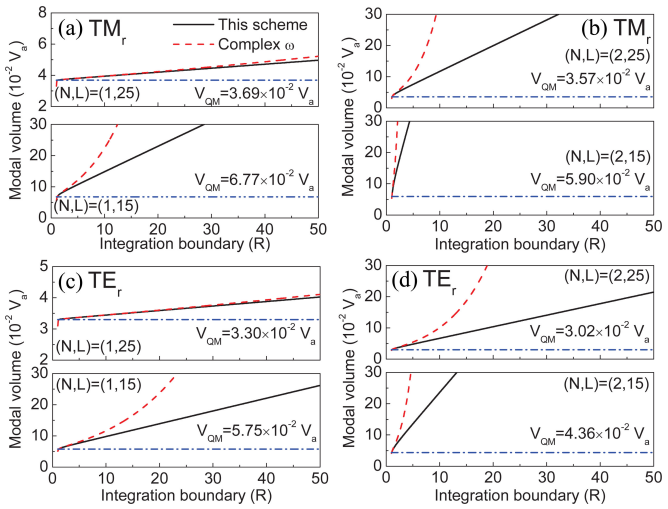

Fig. 8. The modal volume $V_{\mathrm{QM},l}$ and its indefinite counterparts as a function of R_b for (a) TM_r WGMs with $N=1$, (b) TM_r WGMs with $N=2$, (c) TE_r WGMs with $N=1$, and (d) TE_r WGMs with $N=2$ (identical line styles to those in Fig. 6). The indefinite counterparts of $V_{\mathrm{QM},l}$s diverge as R_b increases. For the complex-ω method, the effect of divergence takes place at the smaller R_b than that based on the current scheme. The discrepancy is more significant for the low-Q modes.

energy confinement factors based on the complex-ω method is more stringent for low-Q modes.

The modal volume V_QM and its indefinite counterparts as a function of the integration boundary [see (16b)] are shown in Fig. 8. The trends of indefinite modal volumes are opposite to those of conventional energy confinement factors $\Gamma_{\mathrm{E},l}^{(\mathrm{old})}(\Omega)$. For high-$Q$ WGMs, the deviations of indefinite modal volumes from $V_{\mathrm{QM},l}$ [upper graphs of Fig. 8(a) and (c)] are milder than those of low-Q modes. Quantitatively, in the range of R_b considered here, the indefinite modal volumes based on the mode profiles from the current scheme and complex-ω method are similar for high-Q modes, but those of the low-Q modes are significantly different. With the complex-ω method, the indefinite modal volume diverges more rapidly as the Q factor becomes lower due to the exponential growth $\exp[\omega_l r/(2cQ_l)]$ of the field in the free space. These features indicate that estimations of V_QM based on field integrations and complex-ω method [15] are acceptable if (1) the target mode has a high radiative Q factor, and (2) the integration does not extend much into the far-field zone. However, the uncertainty due to integration regions is never fully eliminated and may become significant as radiative Q factors decrease. On the other hand, without the knowledge of radiative Q factors and specification of integration regions, the indefiniteness can be always eliminated with the calculations of $\Gamma_{\mathrm{E},l}$ in (9) [together with (7) and $\Delta\epsilon_{\mathrm{r},l,\mathrm{I}}(\omega_l)$], $V_{\mathrm{eff},l}$ in (16a), and $V_{\mathrm{QM},l}$ in (16b).

VI. Conclusion

We have presented a self-consistent approach to calculate confinement factors and modal volumes. This scheme does not require numerical integrations of fields and is free from the indefiniteness originated from choices of integration regions. The field representations of confinement factors and modal volumes derived from this method indicate that the irrelevant contribution to matter–field interactions from the far field is automatically eliminated by the built-in counter terms. This feature is particularly suitable for modes with low radiative Q factors and small cavities without sharp borders or optical feedback structures. The simple formulae for these physical parameters are useful for applications of micro- and nanocavities such as lasers, cavity QED, and Purcell effect.

Appendix A
Simplification for Field Representation of Confinement Factor

Some arbitrariness needs to be fixed for the fields $\mathbf{p}_l(\mathbf{r})$ and $\mathbf{q}_l(\mathbf{r})$. If $\mathbf{f}_l(\mathbf{r},\omega)$ is the solution of the generalized eigenvalue problem in (6a), the field $\hat{\mathbf{f}}_l(\mathbf{r},\omega)$ defined as

$$\hat{\mathbf{f}}_l(\mathbf{r},\omega) \equiv h_l(\omega)\mathbf{f}_l(\mathbf{r},\omega) \tag{19a}$$

also satisfies the same generalized eigenvalue problem with the same permittivity variation $\Delta\epsilon_{\mathrm{r},l}(\omega)$, where $h_l(\omega)$ is a frequency-dependent complex number for mode l. If we define a new set of fields $\hat{\mathbf{g}}_l(\mathbf{r},\omega)$, $\hat{\mathbf{p}}_l(\mathbf{r})$, and $\hat{\mathbf{q}}_l(\mathbf{r})$ for $\mathbf{g}_l(\mathbf{r},\omega)$, $\mathbf{p}_l(\mathbf{r})$, and $\mathbf{q}_l(\mathbf{r})$, respectively, as follows:

$$\hat{\mathbf{g}}_l(\mathbf{r},\omega) \equiv h_l(\omega)\mathbf{g}_l(\mathbf{r},\omega) \tag{19b}$$

$$\begin{aligned}\hat{\mathbf{p}}_l(\mathbf{r}) &\equiv \omega_l \frac{\partial \hat{\mathbf{f}}_l(\mathbf{r},\omega)}{\partial\omega}\bigg|_{\omega=\omega_l} \\ &= h_l(\omega_l)\mathbf{p}_l(\mathbf{r}) + \omega_l h_l'(\omega_l)\mathbf{f}_l(\mathbf{r},\omega_l)\end{aligned} \tag{19c}$$

$$\begin{aligned}\hat{\mathbf{q}}_l(\mathbf{r}) &\equiv \frac{1}{i\omega_l\mu_0}\nabla\times\hat{\mathbf{p}}_l(\mathbf{r}) \\ &= h_l(\omega_l)\mathbf{q}_l(\mathbf{r}) + \omega_l h_l'(\omega_l)\mathbf{g}_l(\mathbf{r},\omega_l)\end{aligned} \tag{19d}$$

where $h_l'(\omega) = \mathrm{d}h_l(\omega)/\mathrm{d}\omega$, it can be shown that with the real part of Poynting's theorem at ω_l:

$$\begin{aligned}0 = &\oint_S \mathrm{d}\mathbf{a}\cdot\mathrm{Re}\left[\frac{\mathbf{f}_l(\mathbf{r},\omega_l)\times\mathbf{g}_l^*(\mathbf{r},\omega_l)}{2}\right] \\ &+ \frac{\omega_l\epsilon_0}{2}\int_\Omega \mathrm{d}\mathbf{r}\mathbf{f}_l(\mathbf{r},\omega_l)\cdot\bar{\bar{\epsilon}}_{\mathrm{r,I}}(\mathbf{r},\omega_l)\mathbf{f}_l^*(\mathbf{r},\omega_l) \\ &+ \frac{\omega_l\epsilon_0\Delta\epsilon_{\mathrm{r},l,\mathrm{I}}(\omega_l)}{2}\int_{\Omega_\mathrm{a}}\mathrm{d}\mathbf{r}|\mathbf{f}_l(\mathbf{r},\omega_l)|^2.\end{aligned} \tag{20}$$

Q_l and $\Gamma_{\mathrm{E},l}$ in (13) and (14), respectively, are invariant to the transformation in (19a) to (19d). The solution of $\mathbf{p}_l(\mathbf{r})$ is not unique unless some constraint is specified. This situation reflects that the differential operator in (11) has the homogeneous solution of $\mathbf{f}_l(\mathbf{r},\omega_l)$.

In fact, we can fix the fields in (19a)–(19d) by imposing particular normalization schemes to $\mathbf{f}_l(\mathbf{r},\omega)$ and simplify the field representations of Q_l and $\Gamma_{\mathrm{E},l}$. For example, we may pick up the following pair of conditions:

$$\int_{\Omega_\mathrm{a}}\mathrm{d}\mathbf{r}|\mathbf{f}_l(\mathbf{r},\omega)|^2 = \zeta_l(\omega)\in\mathbb{R}^+ \tag{21a}$$

$$\int_{\Omega_\mathrm{a}} \mathrm{d}\mathbf{r}\mathbf{f}_l^*(\mathbf{r},\omega_l)\cdot\mathbf{f}_l(\mathbf{r},\omega) = \xi_l(\omega)\in\mathbb{R}^+ \tag{21b}$$

where $\zeta_l(\omega)$ is a positive and frequency-dependent factor given in advance; and $\xi_l(\omega)$ is determined after the positiveness of (21a) is enforced [note that $\zeta_l(\omega_l)=\xi_l(\omega_l)$]. The condition in (21b) simplifies the field representations of Q_l and $\Gamma_{\mathrm{E},l}$ in (13) and (14), respectively. We first take the frequency derivative on both sides of (21b):

$$\omega\frac{\mathrm{d}}{\mathrm{d}\omega}\left[\int_{\Omega_\mathrm{a}}\mathrm{d}\mathbf{r}\mathbf{f}_l^*(\mathbf{r},\omega_l)\cdot\mathbf{f}_l(\mathbf{r},\omega)\right]_{\omega=\omega_l} = \int_{\Omega_\mathrm{a}}\mathrm{d}\mathbf{r}\mathbf{f}_l^*(\mathbf{r},\omega_l)\cdot\mathbf{p}_l(\mathbf{r}) = \omega_l\xi_l'(\omega_l)\in\mathbb{R}^+. \tag{22}$$

After taking the imaginary part on the second line of (22), we obtain a useful null identity:

$$\int_{\Omega_\mathrm{a}}\mathrm{d}\mathbf{r}\mathrm{Im}[\mathbf{f}_l^*(\mathbf{r},\omega_l)\cdot\mathbf{p}_l(\mathbf{r},\omega_l)] = 0. \tag{23}$$

The LHS of (23) appears on the third line of (13) (Q_l) and the fourth line of (14) ($\Gamma_{\mathrm{E},l}$). With the normalization conditions in (21a) and (21b), we can drop these terms in (13) and (14). If we further set $\Omega=\Omega_\mathrm{a}$ and $S=S_\mathrm{a}$, we may drop more terms due to the homogeneous and isotropic active region and (23), and compactly express Q_l and $\Gamma_{\mathrm{E},l}$ as

$$Q_l = -\frac{[\epsilon_{\mathrm{g,a}}(\omega_l)+\epsilon_{\mathrm{a,R}}(\omega_l)]}{2\Delta\epsilon_{\mathrm{r},l,\mathrm{I}}(\omega_l)} - \frac{\Delta\epsilon_{\mathrm{r},l,\mathrm{R}}(\omega_l)}{2\Delta\epsilon_{\mathrm{r},l,\mathrm{I}}(\omega_l)} - \frac{\frac{1}{\omega_l\epsilon_0}\oint_{S_\mathrm{a}}\mathrm{d}\mathbf{a}\cdot\mathrm{Im}[\mathbf{q}_l(\mathbf{r})\times\mathbf{f}_l^*(\mathbf{r},\omega_l)-\mathbf{p}_l(\mathbf{r})\times\mathbf{g}_l^*(\mathbf{r},\omega_l)]}{2\Delta\epsilon_{\mathrm{r},l,\mathrm{I}}(\omega_l)\int_{\Omega_\mathrm{a}}\mathrm{d}\mathbf{r}|\mathbf{f}_l(\mathbf{r},\omega_l)|^2} \tag{24}$$

$$\frac{1}{\Gamma_{\mathrm{E},l}} \approx 1 + \frac{\Delta\epsilon_{\mathrm{r},l,\mathrm{R}}(\omega_l)}{[\epsilon_{\mathrm{g,a}}(\omega_l)+\epsilon_{\mathrm{a,R}}(\omega_l)]} + \frac{\frac{1}{4\omega_l}\oint_{S_\mathrm{a}}\mathrm{d}\mathbf{a}\cdot\mathrm{Im}[\mathbf{q}_l(\mathbf{r})\times\mathbf{f}_l^*(\mathbf{r},\omega_l)-\mathbf{p}_l(\mathbf{r})\times\mathbf{g}_l^*(\mathbf{r},\omega_l)]}{\int_{\Omega_\mathrm{a}}\mathrm{d}\mathbf{r}\frac{\epsilon_0}{4}[\epsilon_{\mathrm{g,a}}(\omega_l)+\epsilon_{\mathrm{a,R}}(\omega_l)]|\mathbf{f}_l(\mathbf{r},\omega_l)|^2}. \tag{25}$$

Appendix B
Invariance of Field Representation of Confinement Factor to Integration Regions

We prove the invariance of the field representation in (14) by showing that $\Gamma_{\mathrm{E},l}^{-1}$s evaluated with any integration regions that contain Ω_a are all identical to a single value. For an arbitrary integration region Ω_1 ($\Omega_\mathrm{a}\subseteq\Omega_1$) and its surface S_1, let us check the difference of $\Gamma_{\mathrm{E},l}^{-1}$s which are evaluated with $(\Omega,S)=(\Omega_1,S_1)$ and $(\Omega,S)=(\Omega_\mathrm{a},S_\mathrm{a})$ in (14), respectively:

$$\left.\frac{1}{\Gamma_{\mathrm{E},l}}\right|_{(\Omega,S)=(\Omega_1,S_1)} - \left.\frac{1}{\Gamma_{\mathrm{E},l}}\right|_{(\Omega,S)=(\Omega_\mathrm{a},S_\mathrm{a})} = \frac{1}{\omega_l\int_{\Omega_\mathrm{a}}\mathrm{d}\mathbf{r}\frac{\epsilon_0}{2}[\epsilon_{\mathrm{g,a}}(\omega_l)+\epsilon_{\mathrm{a,R}}(\omega_l)]|\mathbf{f}_l(\mathbf{r},\omega_l)|^2}$$
$$\times\left\{\omega_l\int_{\Omega_1'}\mathrm{d}\mathbf{r}\mathbf{f}_l^*(\mathbf{r},\omega_l)\cdot\frac{\epsilon_0}{2}\left[\overline{\overline{\epsilon}}_\mathrm{g}(\mathbf{r},\omega_l)+\overline{\overline{\epsilon}}_{\mathrm{r,R}}(\mathbf{r},\omega_l)\right]\mathbf{f}_l(\mathbf{r},\omega_l)\right.$$
$$-\omega_l\int_{\Omega_1'}\mathrm{d}\mathbf{r}\epsilon_0\mathrm{Im}\left[\mathbf{f}_l^*(\mathbf{r},\omega_l)\cdot\overline{\overline{\epsilon}}_{\mathrm{r,I}}(\mathbf{r},\omega_l)\mathbf{p}_l(\mathbf{r})\right]$$
$$\left.+\frac{1}{2}\oint_{S_1'}\mathrm{d}\mathbf{a}\cdot\mathrm{Im}[\mathbf{q}_l(\mathbf{r})\times\mathbf{f}_l^*(\mathbf{r},\omega_l)-\mathbf{p}_l(\mathbf{r})\times\mathbf{g}_l^*(\mathbf{r},\omega_l)]\right\} \tag{26}$$

where $\Omega_1'=\Omega_1-\Omega_\mathrm{a}$ is the region of Ω_1 excluding Ω_a; and $S_1'=S_1\cup S_\mathrm{a}$ is the union of the two surfaces.

From (11), the wave equation of $\mathbf{p}_l(\mathbf{r})$ in Ω_1' becomes

$$\nabla\times\nabla\times\mathbf{p}_l(\mathbf{r}) - \left(\frac{\omega_l}{c}\right)^2\overline{\overline{\epsilon}}_\mathrm{r}(\mathbf{r},\omega_l)\mathbf{p}_l(\mathbf{r}) = i\omega_l\mu_0\mathbf{j}_{\mathrm{eff},l}(\mathbf{r}) \tag{27a}$$

where the effective source $\mathbf{j}_{\mathrm{eff},l}(\mathbf{r})$ is defined as

$$\mathbf{j}_{\mathrm{eff},l}(\mathbf{r}) = -i\omega_l\epsilon_0\left[\overline{\overline{\epsilon}}_\mathrm{g}^{(\mathrm{c})}(\mathbf{r},\omega_l)+\overline{\overline{\epsilon}}_\mathrm{r}(\mathbf{r},\omega_l)\right]\mathbf{f}_l(\mathbf{r},\omega_l). \tag{27b}$$

As indicated in (10b), (27a), and (27b), the fields $\mathbf{p}_l(\mathbf{r})$ and $\mathbf{q}_l(\mathbf{r})$ and effective source $\mathbf{j}_{\mathrm{eff},l}(\mathbf{r})$ satisfy Maxwell's equations in Ω_1'. On the other hand, the fields $\mathbf{f}_l(\mathbf{r},\omega_l)$ and $\mathbf{g}_l(\mathbf{r},\omega_l)$ are solutions of the *source-free* Maxwell's equations in Ω_1'. With the generalized Poynting theorem in the frequency domain:

$$\nabla\cdot\frac{1}{2}(\mathbf{E}_1\times\mathbf{H}_2^*) = \frac{i\omega}{2}(\mathbf{H}_2^*\cdot\mathbf{B}_1-\mathbf{E}_1\cdot\mathbf{D}_2^*) - \frac{1}{2}\mathbf{E}_1\cdot\mathbf{J}_{\mathrm{s},2}^* \tag{28a}$$

$$\nabla\cdot\frac{1}{2}(\mathbf{E}_2\times\mathbf{H}_1^*) = \frac{i\omega}{2}(\mathbf{H}_1^*\cdot\mathbf{B}_2-\mathbf{E}_2\cdot\mathbf{D}_1^*) - \frac{1}{2}\mathbf{E}_2\cdot\mathbf{J}_{\mathrm{s},1}^* \tag{28b}$$

where $(\mathbf{E}_1,\mathbf{H}_1,\mathbf{D}_1,\mathbf{B}_1)$ are the electric, magnetic, electric displacement, and magnetic flux fields in the presence of source $\mathbf{J}_{\mathrm{s},1}$, respectively; and $(\mathbf{E}_2,\mathbf{H}_2,\mathbf{D}_2,\mathbf{B}_2)$ are the counterparts in the presence of $\mathbf{J}_{\mathrm{s},2}$; we first add the complex conjugate of (28a) to (28b) and then integrate the outcome over Ω_1'. After utilizing the divergence theorem and taking the imaginary part of the resulted integral, we obtain the following identity:

$$\begin{aligned}0 = &-\int_{\Omega_1'}\mathrm{d}\mathbf{r}\frac{1}{2}\mathrm{Im}\left[\mathbf{E}_1^*\cdot\mathbf{J}_{\mathrm{s},2}+\mathbf{E}_2\cdot\mathbf{J}_{\mathrm{s},1}^*\right]\\ &-\int_{\Omega_1'}\mathrm{d}\mathbf{r}\frac{\omega}{2}\mathrm{Re}\left[\mathbf{H}_2\cdot\mathbf{B}_1^*-\mathbf{H}_1^*\cdot\mathbf{B}_2\right]\\ &+\int_{\Omega_1'}\mathrm{d}\mathbf{r}\frac{\omega}{2}\mathrm{Re}\left[\mathbf{E}_1^*\cdot\mathbf{D}_2-\mathbf{E}_2\cdot\mathbf{D}_1^*\right]\\ &+\oint_{S_1'}\mathrm{d}\mathbf{a}\cdot\frac{1}{2}\mathrm{Im}\left[\mathbf{H}_2\times\mathbf{E}_1^*-\mathbf{E}_2\times\mathbf{H}_1^*\right].\end{aligned} \tag{29}$$

If we set $\omega=\omega_l$ and assign the fields and sources in Ω_1' as

$$\begin{cases}\mathbf{E}_1=\mathbf{f}_l(\mathbf{r},\omega_l)\\ \mathbf{H}_1=\mathbf{g}_l(\mathbf{r},\omega_l)\\ \mathbf{J}_{\mathrm{s},1}=\mathbf{0}\end{cases}\quad\begin{cases}\mathbf{D}_1=\epsilon_0\,\overline{\overline{\epsilon}}_\mathrm{r}(\mathbf{r},\omega_l)\mathbf{f}_l(\mathbf{r},\omega_l)\\ \mathbf{B}_1=\mu_0\mathbf{g}_l(\mathbf{r},\omega_l)\end{cases} \tag{30a}$$

$$\begin{cases}\mathbf{E}_2=\mathbf{p}_l(\mathbf{r})\\ \mathbf{H}_2=\mathbf{q}_l(\mathbf{r})\\ \mathbf{J}_{\mathrm{s},2}=\mathbf{j}_{\mathrm{eff},l}(\mathbf{r})\end{cases}\quad\begin{cases}\mathbf{D}_2=\epsilon_0\,\overline{\overline{\epsilon}}_\mathrm{r}(\mathbf{r},\omega_l)\mathbf{p}_l(\mathbf{r})\\ \mathbf{B}_2=\mu_0\mathbf{q}_l(\mathbf{r})\end{cases} \tag{30b}$$

the RHS of (29) turns into the content inside the curly brackets of (26), which vanishes according to (29) (the second line on the RHS of (29) does not have a corresponding term in (26) because $\mathbf{H}_2^* \cdot \mathbf{B}_1 - \mathbf{H}_1^* \cdot \mathbf{B}_2$ vanishes in this case). Therefore, the inverse energy confinement factors $\Gamma_{\mathrm{E},l}^{-1}$ evaluated with arbitrary integration regions which contain Ω_a are all identical to that evaluated with $\Omega = \Omega_\mathrm{a}$. This indicates that the field representation of $\Gamma_{\mathrm{E},l}^{-1}$ in (14) is indeed invariant to integration regions Ω that contain Ω_a.

The field representation of $\Gamma_{\mathrm{E},l}^{-1}$ in (14) can also be derived using the integral identity in (29) over an arbitrary integration region Ω containing Ω_a. With analogous field and source assignments in (30a) and (30b) based on full wave equations of $\mathbf{f}_l(\mathbf{r},\omega)$ and $\mathbf{p}_l(\mathbf{r})$ in (6a) and (11), respectively, one first derives the field representation of Q_l and then obtains that of $\Gamma_{\mathrm{E},l}^{-1}$ from (9). Comparing the derivation of $\Gamma_{\mathrm{E},l}^{-1}$ through this approach and aforementioned proof, we see the key to the invariance of $\Gamma_{\mathrm{E},l}^{-1}$ that the source $\mathbf{j}_{\mathrm{s},l}(\mathbf{r},\omega)$ of $\mathbf{f}_l(\mathbf{r},\omega_l)$ in (6a) and its frequency derivative $\partial\mathbf{j}_{\mathrm{s},l}(\mathbf{r},\omega)/\partial\omega$ are merely present in Ω_a but vanish elsewhere.

ACKNOWLEDGMENT

The author appreciates the discussion with Prof. S. L. Chuang at the Department of Electrical and Computer Engineering, University of Illinois at Urbana-Champaign.

REFERENCES

[1] W. W. Anderson, "Mode confinement and gain in junction lasers," *IEEE J. Quantum Electron.*, vol. QE-1, no. 6, pp. 228–236, Sep. 1965.
[2] S. L. Chuang, *Physics of Photonic Devices*, 2nd ed., NJ: Wiley, 2009.
[3] L. A. Coldren and S. W. Corzine, *Diode Lasers and Photonic Integrated Circuits*, 1st ed. New York: Wiley, 1995.
[4] A. Yariv, *Quantum Electronics*, 3rd ed. New York: Wiley, 1989.
[5] T. D. Visser, H. Blok, B. Demeulenaere, and D. Lenstra, "Confinement factors and gain in optical amplifiers," *IEEE J. Quantum Electron.*, vol. 33, no. 10, pp. 1763–1766, Oct. 1997.
[6] A. V. Maslov and C. Z. Ning, "Modal gain in a semiconductor nanowire laser with anisotropic bandstructure," *IEEE J. Quantum Electron.*, vol. 40, no. 10, pp. 1389–1397, Oct. 2004.
[7] C. Manolatou and F. Rana, "Subwavelength nanopatch cavities for semiconductor plasmon lasers," *IEEE J. Quantum. Electron.*, vol. 44, no. 5, pp. 435–447, May 2008.
[8] S. W. Chang and S. L. Chuang, "Fundamental formulation for plasmonic nanolasers," *IEEE J. Quantum. Electron.*, vol. 45, no. 8, pp. 1004–1013, Aug. 2009.
[9] A. Mock, "First principles derivation of microcavity semiconductor laser threshold condition and its application to FDTD active cavity modeling," *J. Opt. Soc. Amer. B*, vol. 27, no. 11, pp. 2262–2272, Nov. 2010.
[10] C. Y. A. Ni, S. W. Chang, D. J. Gargas, M. C. Moore, P. D. Yang, and S. L. Chuang, "Metal-coated zinc oxide nanocavities," *IEEE J. Quantum Electron.*, vol. 47, no. 2, pp. 245–251, Feb. 2011.
[11] J. Huang, S. H. Kim, and A. Scherer, "Design of a surface-emitting, subwavelength metal-clad disk laser in the visible spectrum," *Opt. Exp.*, vol. 18, no. 19, pp. 19 581–19 591, Sep. 2010.
[12] C. Y. Lu and S. L. Chuang, "A surface-emitting 3d metal-nanocavity laser: Proposal and theory," *Opt. Exp.*, vol. 19, no. 14, pp. 13 225–13 244, Jul. 2011.
[13] J. D. Jakson, *Classical Electrodynamics*, 3rd ed. New York: Wiley, 1999.
[14] E. I. Smotrova, V. O. Byelobrov, T. M. Benson, J. Ctyroky, R. Sauleau, and A. I. Nosich, "Optical theorem helps understand thresholds of lasing in microcavities with active regions," *IEEE J. Quantum. Electron.*, vol. 47, no. 1, pp. 20–30, Jan. 2011.
[15] S. M. Spillane, T. J. Kippenberg, K. J. Vahala, K. W. Goh, E. Wilcut, and H. J. Kimble, "Ultrahigh-Q toroidal microresonators for cavity quantum electrodynamics," *Phys. Rev. A*, vol. 71, no. 1, pp. 013817-1–013817-10, Jan. 2005.
[16] A. Nosich, E. Smotrova, S. Boriskina, T. Benson, and P. Sewell, "Trends in microdisk laser research and linear optical modeling," *Opt. Quant. Electron.*, vol. 39, no. 15, pp. 1253–1272, Dec. 2007.
[17] S. W. Chang, "Full frequency-domain approach to reciprocal microlasers and nanolasers—Perspective from Lorentz reciprocity," *Opt. Exp.*, vol. 19, no. 22, pp. 21 116–21 134, Oct. 2011.
[18] J.-M. Gerard and B. Gayral, "Strong Purcell effect for InAs quantum boxes in three-dimensional solid-state microcavities," *J. Lightw. Technol.*, vol. 17, no. 11, pp. 2089–2095, Nov. 1999.
[19] Y. G. Wang, S. W. Chang, C. C. Chen, C. H. Chiu, M. Y. Kuo, M. H. Shih, and H. C. Kuo, "Room temperature lasing with high group index in metal-coated GaN nanoring," *Appl. Phys. Lett.*, vol. 99, no. 25, pp. 251111-1–251111-3, Dec. 2011.
[20] A. V. Maslov and M. Miyawaki, "Confinement factors and optical gain in subwavelength plasmonic resonators," *J. Appl. Phys.*, vol. 108, no. 8, pp. 083105-1–083105-6, Oct. 2010.
[21] M. E. Peskin and D. V. Schroeder, *An Introduction to Quantum Field Theory*, 1st ed. Boulder CO: Westview, 1995.
[22] S. W. Chang and S. L. Chuang, "Normal modes for plasmonic nanolasers with dispersive and inhomogeneous media," *Opt. Lett.*, vol. 34, no. 1, pp. 91–93, Jan. 2009.
[23] S. Schiller, "Asymptotic expansion of morphological resonance frequencies in Mie scattering," *Appl. Opt.*, vol. 32, no. 12, pp. 2181–2185, Apr. 1993.
[24] L. A. Weinstein, *Open Resonators and Open Waveguides*. Boulder CO: Golem Press, 1969.
[25] S. M. Spillane, "Fiber-coupled ultra-high-Q microresonators for nonlinear and quantum optics," Ph.D. dissertation, California Inst. Technol., CA, May 2004.
[26] M. H. Huang, S. Mao, H. Feick, H. Yan, Y. Wu, H. Kind, E. Weber, R. Russo, and P. Yang, "Room-temperature ultraviolet nanowire nanolasers," *Science*, vol. 292, no. 5523, pp. 1897–1899, Jun. 2001.
[27] M. A. Zimmler, J. Bao, F. Capasso, S. Müller, and C. Ronning, "Laser action in nanowires: observation of the transition from amplified spontaneous emission to laser oscillation," *Appl. Phys. Lett.*, vol. 93, no. 5, pp. 051101-1–051101-3, Aug. 2008.
[28] D. J. Gargas, M. C. Moore, A. Ni, S. W. Chang, Z. Zhang, S. L. Chuang, and P. Yang, "Whispering gallery mode lasing from zinc oxide hexagonal nanodisks," *ACS Nano*, vol. 4, no. 6, pp. 3270–3276, Apr. 2010.
[29] M. T. Hill, M. Marell, E. S. P. Leong, B. Smalbrugge, Y. Zhu, M. Sun, P. J. van Veldhoven, E. J. Geluk, F. Karouta, Y. S. Oei, R. Nötzel, C. Z. Ning, and M. K. Smit, "Lasing in metal-insulator-metal sub-wavelength plasmonic waveguides," *Opt. Exp.*, vol. 17, no. 13, pp. 11 107–11 112, Jun. 2009.

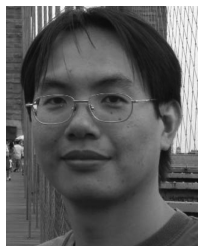

Shu-Wei Chang (M'09) received the B.S. degree in electrical engineering from the National Taiwan University, Taipei, Taiwan, in 1999, and the M.S. and Ph.D. degrees from the University of Illinois at Urbana-Champaign, Urbana, in 2003 and 2006, respectively.

From 2008 to 2010, he was a Postdoctorate Associate at the Department of Electrical and Computer Engineering, University of Illinois at Urbana-Champaign. Since 2010, he has been an Assistant Research Fellow at the Research Center for Applied Sciences, Academia Sinica, Taipei. In 2011, he joined the faculties of the Department of Photonics, National Chiao-Tung University, Hsinchu, Taiwan, as an Adjunct Assistant Professor. His current research interests are fundamental and applied physics of semiconductor photonics including tunneling-injection quantum-dot-quantum-well coupled system, slow and fast light in semiconductor nanostructures, spin relaxation in strained [1 1 0] and [1 1 1] semiconductor quantum wells, group-IV direct-bandgap semiconductor lasers, active and passive plasmonic devices, semiconductor nanolasers, applications of metamaterials, both chiral and nonchiral, to semiconductor active devices, and computational schemes for both reciprocal and nonreciprocal cavities.

Dr. Chang is a member of the Optical Society of America. He was the recipient of the John Bardeen Memorial Graduate Award from the Department of Electrical and Computer Engineering, University of Illinois at Urbana-Champaign, in 2006.